Electron Paramagnetic Resonance Studies of Functionally Active, Nitroxide Spin-Labeled Peptide Analogues of the C-Terminus of a G-Protein α Subunit

ARTICLE *in* BIOCHEMISTRY · AUGUST 2010

Impact Factor: 3.02 · DOI: 10.1021/bi100846c · Source: PubMed

6 AUTHORS, INCLUDING:

Thomas Baranski
Washington University in St. Louis
56 PUBLICATIONS **1,599** CITATIONS
SEE PROFILE

Garland R Marshall
Washington University in St. Louis
376 PUBLICATIONS **10,154** CITATIONS
SEE PROFILE

Published in final edited form as:
Biochemistry. 2010 August 17; 49(32): 6877–6886. doi:10.1021/bi100846c.

EPR Studies of Functionally Active, Nitroxide Spin-Labeled Peptide Analogs of the C-terminus of a G-Protein Alpha Subunit

Ned Van Eps[3,*], **Lori L. Anderson**[1,2,*], **Oleg G. Kisselev**[4], **Thomas J. Baranski**[2], **Wayne L. Hubbell**[3,#], and **Garland R. Marshall**[1,#]

[1]Department of Biochemistry and Molecular Biophysics, Washington University, St. Louis, MO 63110

[2]Departments of Medicine, Molecular Biology and Pharmacology, Washington University, St. Louis, MO 63110

[3]Jules Stein Eye Institute and Department of Chemistry and Biochemistry, University of California, Los Angeles, California 90095-7008

[4]Departments of Ophthalmology and of Biochemistry and Molecular Biology, St. Louis University School of Medicine, St. Louis, MO, 63104

Abstract

The C-terminal tail of the transducin alpha subunit, Gtα(340–350), is known to bind and stabilize the active conformation of rhodopsin upon photoactivation (R*). Five spin-labeled analogs of Gtα(340–350) demonstrated native-like activity in their ability to bind and stabilize R*. The spin label 2,2,6,6-tetramethylpiperidine-1-oxyl-4-amino-4-carboxylic acid (TOAC) was employed at interior sites within the peptide, whereas a Proxyl (3-carboxyl-2,2,5,5-tetramethyl-pyrrolidinyloxy) spin label was employed at the amino terminus of the peptide. Upon binding to R*, the electron paramagnetic resonance spectrum of TOAC^{343}-Gtα(340–350) revealed greater immobilization of the nitroxide when compared to that of the N-terminal modified Proxyl-Gtα(340–350) analog. A double-labeled Proxyl/TOAC^{348}-Gtα(340–350) was examined by DEER spectroscopy to determine the distribution of distances between the two nitroxides in the peptides when in solution and when bound to R*. TOAC and Proxyl spin labels in this GPCR-G-protein α-peptide system provide unique biophysical probes that can be used to explore the structure and conformational changes at the rhodopsin-G-protein interface.

Spin-labeled proteins and peptides, as used in EPR studies, provide a dynamic view of biological phenomenon. In site-directed spin labeling (SDSL), nitroxide amino acids are selectively introduced into a peptide or protein, and the electron paramagnetic resonance is analyzed to provide information on sequence-specific secondary and tertiary structure, membrane protein topography and electrostatic potential (1), conformational changes (2), protein dynamics (3), and inter-nitroxide distances (4–7). In most studies, the nitroxide side chain designated R1 has been employed (Figure 1a). Crystallographic (8–11), mutagenic (12,13) and spectral simulation studies (14) revealed that internal motions of the side chain are constrained due to interactions of the disulfide with main-chain atoms. Thus, the dynamics, and hence the EPR spectra, are primarily determined by limited torsional oscillations about two dihedral angles (angles X_4 and X_5 in Figure 1a). As a result of this constrained motion, the EPR spectrum is highly sensitive to additional backbone

[#]Corresponding authors – GRM, 314-362-1567, no fax, garlandm@gmail.com. [#]WLH, 310-206-8830, 310-794-2144 (fax), hubbellw@jsei.ucla.edu.
[*]These authors contributed equally to the work.

fluctuations and to modulations of the motion due to interactions of the nitroxide with the local environment in the protein. Thus, the EPR spectrum is a “fingerprint” of the local structure and dynamics. For this reason, EPR spectral lineshape analysis of R1 in proteins has been able to reveal and characterize conformational changes (2), in some cases with real time resolution (15–16). Of particular interest for the present report are SDSL studies of receptors systems, including the GPCR rhodopsin (17,18) its cognate G protein transducin (19–23), and the estrogen receptor alpha (24). In addition to investigating conformational changes, EPR spectra of R1 have been analyzed to determine the amplitudes of backbone fluctuations on the nanosecond time scale (3). This is of interest because sequences with flexibility on this time scale often turn out to be involved in protein-protein recognition.

One of the most powerful tools for static structure determination in SDSL is inter-spin distance measurement in systems containing two nitroxide side chains. Under normal physiological temperatures, inter-spin distances in the range of 10–20 Å can readily be measured using continuous wave (CW) EPR deconvolution methods to extract dipolar broadening (4,5). At low temperature, the time-domain method DEER (Double Electron Electron Resonance) extends the distance range to near 80 Å (6,7). Most importantly, DEER resolves multiple discrete distances and their corresponding distributions, with the only disadvantage that time-resolved changes in distances are not readily monitored due to the requirement of low temperature. Thus, the range of distances between 10 – 80 Å is accessible, ideal for mapping structure and structural changes in proteins and complexes.

Although the R1 side chain has proven extremely useful as a monitor of local protein structure and dynamics, the inherent potential for the R1 side chain to adopt multiple rotamers in proteins warrants particular care for interpretation of interspin-distances in terms of protein structure. Despite the fact that R1 has a limited conformational space at solvent-exposed sites (8–11), interactions with the protein can result in the population of higher energy rotamers. This can be mitigated for measuring structural *changes* by judicious selection of sites for R1 introduction (18), but uncertainty remains for relating inter-nitroxide distances to distances between Cα carbons. This uncertainty can be overcome to some extent with sufficient distance constraints to localize the spatial position of the nitroxide, but practical applications requires multiple nitroxide pairs (18).

The present report explores the utility of a more constrained side chain, TOAC (Figure 1b). The tetra-substituted α,α-dialkyl spin label TOAC (2,2,6,6-tetramethylpiperidine-1-oxyl-4-amino-4-carboxylic acid) (25) contains a nitroxide ring attached to the peptide backbone through its α-carbon (Figure 1b). Due to the self-imposed cyclic constraints of TOAC, it provides a useful tool in measuring conformational changes using DEER, since distances between TOACs are not compromised by uncertainties in rotamer distribution, but TOAC does have twist-boat ring conformers in which the 2p orbital of the nitroxide is inclined at different angles with respect to an alpha helix axis (26, 27). The fixed spatial orientations of TOACs can complicate simple distance measurements, but this feature is of potential use in measuring relative orientations of structural elements in a protein (28).

The introduction of TOAC into peptide chemistry allowed the first use of linking a rigid spin label to a growing peptide chain through an amide bond. Although incorporation of TOAC has become common by chemical synthesis due to its high sensitivity for monitoring conformational changes within the peptide scaffold, its use in biologically relevant systems is limited, as it cannot be incorporated biosynthetically and is more difficult to synthetically incorporate in peptide sequences for chemical ligation due to its lower reactivity due to steric hinderance.

Acetyl-TOAC-α-MSH (29) and N-terminal TOAC-derivatives of angiotensin (30,31) and bradykinin (31) demonstrated the first syntheses of spin-labeled peptide hormones which maintained biological activity. Furthermore, a series of three, TOAC-labeled, neuropeptide Y analogs maintained their ability to bind the G-protein coupled receptor Y, demonstrating the ability to obtain structural informational upon binding of the NPY ligand to its receptor (32). Smythe et al were the first to incorporate two TOAC residues into model helical peptides for comparison with EPR studies on the more flexible SDSL label R1 (33,34).

Herein, TOAC-labeled Gα-transducin (Gtα)-terminal peptides are used to probe changes in peptide mobility that accompany binding at the GPCR rhodopsin/G-protein interface. Rhodopsin, the primary visual receptor and the prototype of G-protein-coupled receptors, is one of the best characterized of all GPCRs. Upon photoactivation, rhodopsin forms an active signaling conformation, metarhodopsin II (MII) resulting in interaction with transducin (Gtαβγ), its heterotrimeric G-protein partner. Interaction between Gtαβγ and MII stabilizes the MII state and initiates a signal cascade ultimately leading to nucleotide exchange on Gtα resulting in dissociation of Gtαβγ from the GPCR as Gβγ and Gα-GTP (35,36). A synthetic undecapeptide corresponding to Gtα(340–350) (IKENLKDCGLF) binds to activated rhodopsin and stabilizes the MII state, thus mimicking the effects of transducin itself (37). The structure of the Gtα-peptide bound to photoactivated rhodospin was solved using transferred nuclear Overhauser effect (TrNOE) NMR spectroscopy (38,39).

Results reported by Kisselev *et al*. demonstrated that upon light activation, Gtα(340–350) shifts from a highly disordered conformation to a ordered continuous helix terminated by a C-terminal capping motif, associated with the formation of a unique clustering of residues, namely L344, K345, L349 and F350 (39). Similar structural results were obtained by Koenig et al using transferred NOE on an analog of Gtα(340–350) bound to MII (40) as well as by the crystal structure of the undecapeptide bound to opsin (41). The conformational changes that occur in the C-terminal sequence upon receptor interaction were further investigated by fluorescence and spin labeling of substituted cysteines in the Gtα subunit (42,43). Further understanding these conformational changes should provide better insight into possible mechanisms of nucleotide exchange of α-subunits of G-proteins.

Here, the syntheses of spin-labeled Gα peptide analogs, $TOAC^{343}$-Gtα(340–350) and Proxyl-Gtα(340–350) and the double-labeled Proxyl/$TOAC^{348}$-Gtα(340–350) are reported. Each retained the ability to stabilize the MII state of rhodopsin. In addition, the analogous [$TOAC^{343}$] and Proxyl analogs of the 100-fold higher-affinity peptide (VLEDLKSCGLF) reported from phage display (44) were prepared. Finally, the light-dependent binding of these analogs to native rhodopsin in disk membranes was demonstrated.

MATERIALS AND METHODS

Peptide Synthesis

Native Gtα(340–350) IKENLKDCGLF was synthesized in 0.2 mmol scale by manual Fmoc-protection strategy using Fmoc-Phe-Wang resin and the following Fmoc amino acid derivatives: Fmoc-Lys(Boc), Fmoc-Glu(tBu), Fmoc-Asn(Trt), Fmoc-Asp(tBu), and Fmoc-Cys(Trt). Couplings were facilitated by 2-(1H-benzotriazole-1-yl)-1,1,3,3-tetramethyluronium hexafluorophosphate (HBTU) in the presence of DIPEA in DMF, with a 3-fold excess over the amino component. Crude peptide was released from the Wang resin using Reagent K (82.5% trifluoroacetic acid, 5% water, 5% thioanisole, 5% phenol and 2.5% 1,2,-ethanedithiol). After reacting for 1 hour, the mixture was filtered, washed with TFA, evaporated and the crude peptide was precipitated with diethyl ether. The peptide was purified by preparative HPLC using a C-18 column with a 10–90% gradient (solvent A: 0.5% TFA in H_2O; solvent B: 0.038% TFA/90% acetonitrile/10% H_2O) over 25 minutes.

Characterization by MALDI mass spectroscopy gave the expected molecular weight (m/z) of 1279.53.

The synthesis of TOAC^{343}-Gtα(340–350) IKE-TOAC-LKDCGLF and the respective high-affinity analog VLE-TOAC-LKSVGLF followed the same synthesis as above with the following modifications. The stable nitroxide Fmoc-amino acid TOAC was synthesized according to a reported procedure (46). The coupling steps involving the carboxyl and amino groups of TOAC were achieved with 5 eq of Fmoc-amino acid activated by 5 eq of TFFH and 10 eq of DIPEA and repeated twice for 2 hours. After incorporation of TOAC and Asp, unreacted amino groups were acetylated with acetic anhydride/DMF using a catalytic amount of DMAP for 30 minutes. The peptide was cleaved from the resin using HF in the presence of 5% anisole. Following cleavage, the peptide was precipitated with ether, filtered, and extracted with 30% acetic acid and water. The crude peptide was submitted to alkaline treatment (0.02 M ammonium acetate, pH 9, 3 h) to recover the paramagnetic moiety. The peptide was purified by preparative HPLC using a linear gradient of 10–90% B over 26 minutes with solvent A as 0.05 M ammonium acetate, pH 5 and solvent B as 90% acetonitrile. Characterization by electrospray ionization mass spectroscopy gave the expected molecular mass of 1363 and 1302 for the low-and high-affinity analogs respectively.

Proxyl-Gtα(340–350), its respective high-affinity analog and the double-labeled Proxyl/TOAC^{348}-Gtα(340–350) were synthesized through coupling of 3-carboxy-Proxyl (3-carboxyl-2,2,5,5-tetramethyl-pyrrolidinyloxy, Aldrich, St. Louis, MO) to the amino terminus of the peptide sequences as synthesized above. Activation of the carboxyl group of Proxyl (5 eq) was achieved with 5 eq TFFH and 10 eq DIEA and followed by coupling twice for 2 hours. Cleavage and purification was the same as for TOAC^{343}-Gtα(340–350). Analysis by electrospray ionization gave the expected molecular mass of 1448 and 1388 for the low- and high-affinity analogs and 1531 for the double-labeled peptide, respectively.

Preparation of Rod Outer Segments

Urea-washed rod outer segments (ROS) were prepared from dark-adapted retinas (W.L. Lawson Co., Lincoln, NE) using a sucrose-gradient procedure as previously described (46). All purification steps were carried out in dim red light (Kodak safelight filter, 650 nm cutoff) at 4°C. The final ROS samples were resuspended in a 20 mM MES buffer (pH 6.8) containing 100 mM NaCl, 2 mM $MgCl_2$, and 10% glycerol and stored at −80 degrees Celsius until further use.

UV/visible spectroscopy

The binding affinities of Gtα(340–350), TOAC^{343}-Gtα(340–350) and the double-labeled Proxyl/TOAC^{348}-Gtα(340–350) to rhodopsin in rod outer segments (ROS) were measured using a Meta II stabilization assay (47) by UV/visible spectroscopy. The samples contained 2.5 μM rhodopsin in ROS membranes (48) and peptides in buffer A (20 mM Tris-HCl pH 8.0, 130 mM NaCl, 1 mM $MgCl_2$, 1 μM EDTA). The samples were kept on ice and prepared under dim red light to avoid premature bleaching of rhodopsin. The absorption spectrum of dark-adapted rhodopsin was taken, illuminated with 490 ± 5 nm light for 20 s, followed by acquisition of the light-activated spectrum, using a Cary50 spectrophotometer (Varian, Palo Alto, CA). The cuvette compartment was maintained at 4° C. The measurements were done in triplicate at varying peptide concentrations from 1 μM to 5 mM. The Meta II stabilization was calculated as $\Delta A_{380\ nm} - \Delta A_{417\ nm}$, where ΔA is the absorbance change before and after light activation. The data was fit using the equation MII = Baseline + Range * {[peptide] / ([peptide] + EC50)} to obtain EC50 values of the peptides. Baseline and Range values were kept constant throughout all determinations at 0.05 and 0.75, respectively.

EPR Measurements

EPR measurements were carried out on a Bruker 580 spectrometer at X-band microwave frequencies using a high-sensitivity resonator (HS0118) with an optical port. Spin-labeled peptides were mixed with dark-adapted ROS in 20 mM MES buffer (pH 6.8) containing 100 mM NaCl, 2 mM $MgCl_2$, and 10% glycerol and loaded into a quartz flat cell. Low-affinity peptide data were recorded at 277 K to slow the disappearance of the rhodopsin bound component (see discussion below), while high-affinity peptide data were recorded at 296 K. Spectra were initially recorded under dim red light. Samples were subsequently photobleached with a tungsten lamp (500 nm cutoff filter) for 40 s and an EPR spectrum was recorded.

Time-resolved EPR photolysis experiments were initiated with a ~6 ns laser pulse (500 nm) from a Q-switched Nd:YAG laser coupled with a tunable optical paramagnetic oscillator (Vibrant, Opotek, Inc., Carlsbad, CA). The magnetic field position was set at the center field trough of the unbound peptide spectrum, and the resulting EPR transient was detected with 100kHz field modulation. The signals were recorded with a LeCroy digital oscilloscope (LeCroy Corp., Chestnut Ridge, NY).

Double Electron-Electron Resonance Experiments (DEER)

Double spin-labeled peptides were mixed with dark-adapted ROS (both in 10% (v/v) glycerol) and flash frozen in the dark in 1.5 mm × 1.8 mm quartz capillaries in liquid nitrogen. DEER measurements were performed at 50 K on a Bruker Elexsys 580 spectromenter with a 2-mm split-ring resonator. Four-pulsed DEER was carried out as previously described (7,49) with the π pump pulse (16 ns) positioned at the absorption maximum of the field swept spectrum. The observer π (16 ns) and π/2 (8 ns) pulses were positioned at the low-field line of the spectrum (Δf = 70 MHz). After dark-state data were acquired, the samples were thawed, illuminated with light (500-nm-cutoff filter) and refrozen in liquid nitrogen for a second DEER experiment. All DEER data were analyzed with the DEER Analysis 2009 software package freely available at the website http://www.epr.ethz.ch/. Tikhonov regulatization and distance distribution widths were optimized using L-curve analysis implemented in the software package.

RESULTS

Peptide Synthesis

It has been demonstrated that positions that accept Aib (α-aminobutyric acid), will usually also accept TOAC substitutions. Molecular modeling of conformationally constrained peptides identified the analog of Gtα(340–350), AibKAibAibLKDCGLG, that was synthesized and shown to maintain full activity in stabilization of the MII state of rhodopsin (50). Given that Aib mimics the conformational effect of TOAC substitutions on the peptide backbone (51–54), these results suggested that residues I340, E342 and N343 are capable of tolerating substitution. For the work outlined here, we chose substitution with TOAC at N343. A TOAC scan of the C-terminal tail also revealed that substitution of Gly348 with TOAC maintained the ability to stabilize the MII state of rhodopsin (data not shown) and double-labeled Gtα(340–350) Proxyl/$TOAC^{348}$-Gtα(340–350) was therefore prepared.

Binding of spin-labeled Gα peptides to light-activated rhodopsin

EPR studies have focused on characterizing the $TOAC^{343}$-Gtα(340–350) (IKE-TOAC-LKDCGLF; Fig. 1D bottom) and the corresponding high-affinity $TOAC^{343}$ analog (VLE-TOAC-LKSVGLF) in terms of mobility both in the rhodopsin-bound and unbound forms. Characterization of $Proxyl^{340}$-Gtα(340–350) (Figure 1D top) and the corresponding high-affinity analog has also been carried out for comparison with the TOAC analogs. The EPR

spectra of the spin-labeled peptides in the presence of dark- and light-activated ROS membranes are shown in Figure 2. In each case, the spectrum of the peptide in the presence of ROS membranes in the dark is the same as that for the peptide in buffer, and consists of a single component of three relatively sharp lines, characteristic of a rapidly and isotropically tumbling nitroxide (Figure 2, left-hand panel). On the other hand, spectra of the peptides in the presence of photoactivated ROS membranes are a composite of two distinct components (Figure 2, center panel), one of which corresponds to the free peptide in solution. The other component is identified by well-resolved hyperfine extrema (arrows, Figure 2) indicative of peptide immobilization and rhodopsin binding. As expected, the amplitude of the bound component is much greater for the high-affinity analogs. The individual components, resolved by spectral subtraction, are shown for each peptide in the right-hand panel of Figure 2. The components corresponding to the bound states (right panel, blue traces) each have line shapes characteristic of highly immobilized nitroxides. A comparison of the spectral components corresponding to the bound states reveals different mobilities for the TOAC and Proxyl analogs. An approximate rotational correlation time (τ_c) for a nitroxide may be computed from the separation of the outer hyperfine extrema ($2A_{zz}$) and that for the same sample in a frozen state in the absence of motion ($2A_{zz}^0$) (55). For the TOAC and Proxyl analogs of the high-affinity peptide bound to photoactivated rhodopsin, 2Azz is 69 and 64 Gauss, respectively (Figure 2). For both analogs bound to photoactivated rhodopsin, $2Azz^0$ obtained at 223° K is 74 G (spectra not shown), indicating that the nitroxides in each case are located in a polar environment, presumably facing the solvent. From these values, assuming Brownian motion, τ_c is estimated to be 19.4 and 8.7 ns for the TOAC and Proxyl analogs, respectively. Thus, the TOAC analog of the high-affinity peptide is more immobilized than the corresponding Proxyl analog. Because the rotational diffusion of rhodopsin in the disc is very slow ($\tau_R \approx 12\mu s$, (56)), and because TOAC is rigidly attached to the peptide backbone, the 19.4 ns correlation time for the TOAC analog directly measures the fluctuation frequency of the peptide in the rhodopsin binding site. Differences in 2Azz, and hence mobility are observed between TOAC and Proxyl in both the low- affinity and high-affinity peptides.

Activity of the Peptides: Stabilization of MII

The binding of a C-terminal G-alpha peptide or analog to photoactivated rhodopsin can be monitored by an increase in the amount of MII due to the presence of the peptide. A dose-response curve of concentration of peptide relative to its effect on MII stabilization can be fit to the model described in Methods to provide a value for the apparent dissociation constant (Kd). Results are compared for the native Gtα(340–350), the $TOAC^{343}$-Gtα(340–350) and Proxyl-Gtα(340–350) in Figure 1E. The data reveal that the presence of the $TOAC^{343}$ or the Proxyl groups has little effect on the binding affinity to the receptor. Figure 3B shows examples for the $TOAC^{343}$-Gtα(340–350) high-affinity peptide compared with the high-affinity peptide without TOAC. The fits to the data, shown by the solid traces, give Kd values of 10μM and 4.2μM, respectively. Thus, the presence of the TOAC spin label at 343 increases the Kd by about a factor of ≈2.5, corresponding to a modest increase in the free energy of the bound state by 0.5 kCal/mole due to the TOAC.

It is of interest to compare the apparent dissociation constant for a spin-labeled peptide determined by the MII stabilization assay with that determined from direct binding using EPR. Figure 3A, left-hand panel, shows the absorption EPR spectrum (obtained by integration of the first derivative spectra) corresponding to the equilibrium of $TOAC^{343}$-Gtα(340–350) high-affinity peptide with photoactivated rhodopsin (black trace). Also shown are the individual components corresponding to the bound and free peptide (red and green traces, respectively), obtained by subtraction. Integration of the individual spectra provides the relative equilibrium concentrations of each, which gives a K_d of 12.5 μM for the

TOAC^{343}-Gtα(340–350) high-affinity peptide. This compares favorably with the value of 10 μM obtained from the MII stabilization data shown in Figure 3B. Figure 3A, right-hand panel, shows similar data for Proxyl-Gtα(340–350) high-affinity peptide, giving a K_d of 4 μM. This value is essentially identical to that obtained for the non-labeled high-affinity analog using the MII stabilization assay, suggesting that the terminal location of the spin label does not perturb the peptide-R* interaction. Interestingly, the peptide dissociation constants measured in Figure 3A via EPR techniques did not vary over a pH range of 6–8 (data not shown).

Kinetics of binding for Gα peptide analogs

The kinetics of binding to photoactivated rhodopsin (R*) for the TOAC^{343}-Gtα(340–350) high-affinity peptide was determined by monitoring the EPR signal after a ~6 ns actinic flash at 500 nm. Figure 4A shows the EPR spectral amplitude collected at three different peptide concentrations (gray, green, and red traces) monitored at the centerfield trough of the EPR spectrum, corresponding to the unbound peptide (see Figure 2A, right panel). Data was collected as a function of time after the laser pulse and was fit to a single exponential rise (black line) with an apparent lifetime of ~6 ms. The time course of peptide binding was independent of the peptide concentration for the three concentrations tested, suggesting that the binding event is rate limited by structural changes within the rhodopsin photoreceptor that lead to opening of the binding site rather than diffusion of the peptide to the receptor. The data were collected under either pseudo-first order (2.5 mM peptide) or second order (50 and 250 μM peptide) conditions. The second order reaction, however, is not a simple second order binding event, but instead is coupled to the unimolecular appearance of the active receptor state. Figure 4B shows EPR absorption spectra collected as a function of time after the initial rapid-binding event. As is evident, the broad spectral component, corresponding to the bound peptide, decreases in time with a concomitant increase in the sharp component, reflecting a slow, spontaneous, dissociation of the bound peptide from R*. The decay of the bound signal can be fit with a single exponential with half-life of 8 minutes (Figure 4D, open circles), similar to that for MII decay in native disk membranes (57).

Similar results were obtained for the dissociation of the Proxyl-Gtα(340–350) high-affinity peptide from R* (Figure 4C), and the data are included in the plot of Figure 4D (triangles). These results further demonstrate the functionality of the spin-labeled Gtα(340–350) analogs in their ability to bind and stabilize R* and to sense the activated conformational state of the receptor.

DEER spectroscopy

To investigate the conformation of the peptide bound to MII, the high affinity analog of double-labeled Proxyl/TOAC^{348}-Gtα(340–350) (Figure 5A) was prepared so that the distribution of inter-spin distances in the peptide (in solution or when bound to R*) could be monitored by DEER spectroscopy. The Kd of this peptide was 65 μM, and, as expected the EPR spectra of the unbound and bound peptides reflected rapid isotropic motion and strong immobilization, respectively, similar to the spectra of the peptides containing a single nitroxide (Figure 5B). The featureless dipolar evolution function of the peptide in the presence of dark rhodopsin (Figure 5C, upper trace) and the corresponding dipolar spectrum (Figure 5D, black trace) reflect a broad distribution of inter-nitroxide distances in the range 18 to 34 Å, (Figure 5E, black trace), consistent with an ensemble of conformations for the unbound peptide. Distance distributions of peaks longer than 34 Å in Figure 5E are inaccurately determined due to the 1.1 μs length of the dipolar evolution functions. On the other hand, in the presence of R* striking oscillations are evident in the dipolar evolution function (Figure 5C, lower trace) corresponding to a remarkably narrow interspin distance distribution centered at 19Å (Figure 5E, red trace). Modeling of the nitroxides in the crystal

structure conformation of the peptide (41) (Figure 5F) shows this distance to be consistent with the crystal structure and the unique configuration of the R*-bound $G_{t\alpha}$(340–350) as determined by Kisselev et al. from NMR (39).

DISCUSSION

Heterotrimeric α-subunits have been shown to have several contact regions that are critical for receptor interaction (19,58). One of these regions is apparently the C-terminal sequence of Gα, as shown by the fact that a synthetic undecapeptide corresponding to Gtα(340–350) binds to R* and stabilizes the MII state, thus mimicking the effects of transducin itself (37).

In this study, we provide evidence that five spin-labeled Gtα(340–350) analogs maintain their ability to bind and stabilize the photoactivated MII state of rhodopsin. Receptor binding was detected by immobilization of incorporated TOAC and Proxyl residues as the peptide adopts a highly restricted bound conformation. Comparison between the peptide analogs revealed a higher degree of immobilization with the TOAC compared to the Proxyl analog. The difference in immobilization can be explained in part by the fact that the N-terminal Proxyl label is connected by an amide linkage to the Gtα(340–350) backbone, and thus potentially has two additional rotational degrees of freedom relative to TOAC. TOAC is incorporated directly within the peptide chain and has only limited internal motion relative to the backbone. Hence, when the peptide is immobilized on R*, so is the TOAC nitroxide. Interestingly, however, there is some degree of motion on the ns time scale still present in the bound $TOAC^{343}$-Gtα(340–350) and high-affinity analog that cannot be attributed to R* rotational diffusion. The rotational correlation time of rhodopsin in native disk membranes has been measured to be 20–40 μs (59,60). This motion is too slow to affect the EPR lineshape, which is sensitive to motion in the 100 ps – 100 ns time domain. Thus, the ns motions detected in the bound peptide reflect structural fluctuations of the peptide in the binding site on this time scale. It should be possible to construct approximate partition functions from the distance distributions seen in Figure 5 to estimate the change in entropy of the peptide ligand on binding to photoactivated rhodopsin.

Consistent with the bound conformation of Gtα(340–350) peptides to R* observed by NMR is the crystal structure of the complex of opsin with this undecapeptide (41). The crystal structure helps to further rationalize the differences in nitroxide rotational correlation times of the Proxyl and TOAC adducts (see discussion above). Models of the Proxyl peptide using the crystallographic data show that this label projects outward toward solvent (see Figure 5F). Motion due to the additional rotational degrees of freedom is consistent with the higher mobility of the Proxyl relative to the TOAC nitroxide. Note, however, that the Proxyl is still quite immobilized, presumably due to contacts of the nitroxide ring with nearby side chains in rhodopsin. The $TOAC^{343}$-Gtα(340–350) peptide is also solvent accessible (model not shown), but the internal constraints of this spin label prevent additional nitroxide motion. Finally, a TOAC label placed at position 348 reduced the affinity of the labeled peptide (see Figure 5B), likely because the TOAC-348 residue is predicted to have steric clashes with the receptor near the helix 7/8 region (see Figure 5F).

Studies of peptide binding kinetics to a cognate receptor are an important strategy to explore the mechanism of protein-protein recognition. The kinetics of binding of Gtα(340–350) and the high-affinity analog to R* have been previously investigated at low temperature (1.5 deg C) and high pH (7.9) by monitoring the production of “extra MII” induced by peptide binding (61). An advantage of the EPR method described here is that it is a direct measure of the binding interaction compared to the extra MetaII assay which relies upon changes in chromophore protonation states at a receptor site distant from the receptor/G-protein interface. In addition, physiological temperatures, a wide range of pH values and high

concentrations of native disc membranes can be used in the EPR method to investigate the binding mechanism. The latter point is raised because light scattering artifacts due to high concentration of membrane vesicles can complicate interpretation of optical signals, but present no problem in magnetic resonance detection. Light scattering methods have also been used to measure peptide binding to R*, but this method requires an increase in mass of the peptide, accomplished by fusing the peptide to maltose binding protein (MBP, 42.5 kD) (62). While these fused peptides were shown to bind to rhodopsin in a light-dependent manner, rate data were likely influenced by the presence of MBP due to changes in diffusion constant and, most importantly, to steric constraints on the binding event. It could be argued that the presence of the spin label in the peptide could also modify the binding kinetics, but the similarity of the Kd for the singly labeled and native peptides suggest otherwise.

As shown by the data in Fig. 4, the rate of peptide binding to R* as measured by EPR follows a single exponential time course that is apparently rate limited by conformational changes in rhodopsin that lead to the binding competent state of the receptor. This is consistent with earlier studies which showed fast proton release within rhodopsin upon formation of the peptide/receptor complex (16) in DM micelles. The proton release was rate limited by the appearance of the active receptor state at much lower reagent concentrations than used in the current work verifiying the validity of the rate limiting step approximation. The time constant for binding to rhodopsin in ROS membranes observed here (≈ 6 ms) is in the time window for formation of deprotonated forms of the receptor detected optically at 380nm (MIIa, MIIb, $MIIbH^+$) (63–65); presumably the binding competent state corresponds to one of these intermediates. SDSL data first provided direct evidence that the outward movement of transmembrane helix 6 (TM6) by about 5 Å gives rise to the activated state of the receptor (18,66). The outward movement of TM6 is consistent with generation of a binding pocket for the C-terminal tail of the Gtα subunit (and the corresponding peptides) within the intracellular loops of R*. This model is directly supported by the recent crystal structure of an opsin/Gtα(340–350) peptide (41). It is thus reasonable to speculate that the peptide binding is rate-limited by the movement of TM6. The time constant for TM6 movement following an activating light flash has in fact been measured by SDSL to be ≈2 ms, and was shown to correspond to the formation of MIIb, but this was determined for rhodopsin in micelles of DM where rate constants for interconversion of the intermediates are generally accelerated (16). Future studies will be required to identify the specific intermediate competent for peptide binding in the native membrane.

The ability to synthesize fully active, TOAC-labeled analogs of Gtα(340–350) provides a strategy for mapping the structure of the rhodopsin-peptide complex using distance measurements between pairs of spins, one in the peptide and the other at selected sites throughout the cytoplasmic domain of rhodopsin. Such measurements will determine the relative orientation and position of the bound peptide within the complex, and may identify any additional binding modes of lower affinity. The TOAC spin label is ideally suited for this purpose, because incorporation of α, β, and γ carbons as well as the nitroxide moiety into one heterocyclic structure eliminates rotation about side-chain bonds, effectively fixing the nitroxide relative to the backbone. This is a significant advantage over the more commonly used nitroxide side chains where the possible existence of multiple rotamers complicates the interpretation of interspin distances.

Incorporation of synthetic peptides into a Gα subunit by expressed protein ligation has been demonstrated (67,68), setting the stage for future studies that incorporate a TOAC-labeled Gtα(340–350) peptide into the full-length Gtα. Thus, it would be possible to compare salient structural features of the complex formed with R* by the isolated peptide with that formed by the full-length Gtα. Such studies using the internally constrained TOAC should be able to measure structural heterogeneity at the rhodopsin/transducin interface and explore the effect

of allosteric regulators. Such studies should provide insight into enzymatic mechanisms of transducin activation by R*.

Acknowledgments

This research was supported in part by grants from the Lucille P. Markey Predoctoral Fellowship (to L.L.A.), the Chemistry Biology Interface Pathway T32GM0878 (to L.L.A.); NIH grants GM68460, GM53630, and EY1211301 (to G.R.M.), GM71634 and GM63720 (to T.J.B.), GM63203, EY18107 and RPB (to O.G.K.), EY05216 (to W.L.H.), and the Jules Stein Professorship endowment.

Abbreviations

EPR	electron paramagnetic resonance
TOAC	2,2,6,6-tetramethylpiperidine-1-oxyl-4-amino-4-carboxylic acid
Proxyl	3-carboxyl-2,2,5,5-tetramethyl-pyrrolidinyloxy, free radical
G-protein	heterotrimeric guanine nucleotide binding protein
GPCR	G-protein coupled receptor
DEER	double electron-electron resonance

References

1. Hubbell WL, Gross A, Langen R, Lietzow MA. Recent advances in site-directed spin labeling of proteins. Curr Opin Struct Biol. 1998; 8:649–656. [PubMed: 9818271]
2. Hubbell WL, Cafiso DS, Altenbach C. Identifying conformational changes with site-directed spin labeling. Nat Struct Biol. 2000; 7:735–739. [PubMed: 10966640]
3. Columbus L, Hubbell WL. A new spin on protein dynamics. Trends Biochem Sci. 2002; 27:288–295. [PubMed: 12069788]
4. Rabenstein MD, Shin YK. Determination of the distance between two spin labels attached to a macromolecule. Proc Natl Acad Sci U S A. 1995; 92:8239–8243. [PubMed: 7667275]
5. Altenbach C, Oh KJ, Trabanino RJ, Hideg K, Hubbell WL. Estimation of inter-residue distances in spin labeled proteins at physiological temperatures: experimental strategies and practical limitations. Biochemistry. 2001; 40:15471–15482. [PubMed: 11747422]
6. Jeschke G. Distance measurements in the nanometer range by pulse EPR. Chemphyschem. 2002; 3:927–932. [PubMed: 12503132]
7. Pannier M, Veit S, Godt A, Jeschke G, Spiess HW. Dead-time free measurement of dipole-dipole interactions between electron spins. J Magn Reson. 2000; 142:331–340. [PubMed: 10648151]
8. Langen R, Oh KJ, Cascio D, Hubbell WL. Crystal structures of spin labeled T4 lysozyme mutants: implications for the interpretation of EPR spectra in terms of structure. Biochemistry. 2000; 39:8396–8405. [PubMed: 10913245]
9. Fleissner MR, Cascio D, Hubbell WL. Structural origin of weakly ordered nitroxide motion in spin-labeled proteins. Protein Sci. 2009; 18:893–908. [PubMed: 19384990]
10. Guo Z, Cascio D, Hideg K, Hubbell WL. Structural determinants of nitroxide motion in spin-labeled proteins: solvent-exposed sites in helix B of T4 lysozyme. Protein Sci. 2008; 17:228–239. [PubMed: 18096642]
11. Guo Z, Cascio D, Hideg K, Kalai T, Hubbell WL. Structural determinants of nitroxide motion in spin-labeled proteins: tertiary contact and solvent-inaccessible sites in helix G of T4 lysozyme. Protein Sci. 2007; 16:1069–1086. [PubMed: 17473014]
12. McHaourab HS, Lietzow MA, Hideg K, Hubbell WL. Motion of spin-labeled side chains in T4 lysozyme. Correlation with protein structure and dynamics. Biochemistry. 1996; 35:7692–7704. [PubMed: 8672470]

13. Lietzow MA, Hubbell WL. Motion of spin label side chains in cellular retinol-binding protein: correlation with structure and nearest-neighbor interactions in an antiparallel beta-sheet. Biochemistry. 2004; 43:3137–3151. [PubMed: 15023065]

14. Columbus L, Kalai T, Jeko J, Hideg K, Hubbell WL. Molecular motion of spin labeled side chains in alpha-helices: analysis by variation of side chain structure. Biochemistry. 2001; 40:3828–3846. [PubMed: 11300763]

15. Steinhoff HJ, Mollaaghabaga R, Altenbach C, Hideg K, Krebs M, Khorana HG, Hubbell WL. Time-resolved detection of structural changes during the photocycle of spin-labeled bacteriorhodopsin. Science. 1994; 266:105–107. [PubMed: 7939627]

16. Knierim B, Hofmann KP, Ernst OP, Hubbell WL. Sequence of late molecular events in the activation of rhodopsin. Proc Natl Acad Sci. 2007; 104:20290–20295. [PubMed: 18077356]

17. Hubbell WL, Altenbach C, Hubbell CM, Khorana HG. Rhodopsin structure, dynamics, and activation: a perspective from crystallography, site-directed spin labeling, sulfhydryl reactivity, and disulfide cross-linking. Adv Protein Chem. 2003; 63:243–290. [PubMed: 12629973]

18. Altenbach C, Kusnetzow AK, Ernst OP, Hofmann KP, Hubbell WL. High-resolution distance mapping in rhodopsin reveals the pattern of helix movement due to activation. Proc Natl Acad Sci U S A. 2008; 105:7439–7444. [PubMed: 18490656]

19. Oldham WM, Van Eps N, Preininger AM, Hubbell WL, Hamm HE. Mapping allosteric connections from the receptor to the nucleotide binding pocket of heterotrimeric G proteins. Proc Natl Acad Sci. 2007; 104:7927–7932. [PubMed: 17463080]

20. Van Eps N, Oldham WM, Hamm HE, Hubbell WL. Structural and dynamical changes in an alpha-subunit of a heterotrimeric G protein along the activation pathway. Proc Natl Acad Sci. 2006; 103:16194–16199. [PubMed: 17053066]

21. Oldham WM, Van Eps N, Preininger AM, Hubbell WL, Hamm HE. Mechanism of the receptor-catalyzed activation of heterotrimeric G proteins. Nat Struct Mol Biol. 2006; 13:772–777. [PubMed: 16892066]

22. Preininger AM, Van Eps N, Yu NJ, Medkova M, Hubbell WL, Hamm HE. The myristoylated amino terminus of Galpha(i)(1) plays a critical role in the structure and function of Galpha(i)(1) subunits in solution. Biochemistry. 2003; 42:7931–7941. [PubMed: 12834345]

23. Medkova M, Preininger AM, Yu NJ, Hubbell WL, Hamm HE. Conformational changes in the amino-terminal helix of the G protein alpha(i1) following dissociation from Gbetagamma subunit and activation. Biochemistry. 2002; 41:9962–9972. [PubMed: 12146960]

24. Hurth KM, Nilges MJ, Carlson KE, Tamrazi A, Belford RL, Katzenellenbogen JA. Ligand-induced changes in estrogen receptor conformation as measured by site-directed spin labeling. Biochemistry. 2004; 43:1891–1907. [PubMed: 14967030]

25. Rassat A, Rey P. Nitroxides. XXIII. Preparation d'aminoacides radicalaires et de leurs sels complexes. Bull Soc Chim Fra. 1967:815.

26. Marsh D. Orientation of TOAC amino-acid spin labels in alpha-helices and beta-strands. J Magn Reson. 2006; 180:305–310. [PubMed: 16503176]

27. Crisma M, Deschamps JR, George C, Flippen-Anderson JL, Kaptein B, Broxterman QB, Moretto A, Oancea S, Jost M, Formaggio F, Toniolo C. A topographically and conformationally constrained, spin-labeled, alpha-amino acid: crystallographic characterization in peptides. J Pept Res. 2005; 65:564–579. [PubMed: 15885116]

28. Schiemann O, Cekan P, Margraf D, Prisner TF, Sigurdsson ST. Relative orientation of rigid nitroxides by PELDOR: beyond distance measurements in nucleic acids. Angew Chem Int Ed Engl. 2009; 48:3292–3295. [PubMed: 19322852]

29. Barbosa SR, Cilli EM, Lamy-Freund MT, Castrucci AM, Nakaie CR. First synthesis of a fully active spin-labeled peptide hormone. FEBS Lett. 1999; 446:45–48. [PubMed: 10100612]

30. Vesterman B, Sekacis I, Betins J, Podins L, Nikiforovich GV. Equilibrium of conformers in solution: spin-labelled angiotensin. FEBS Lett. 1985; 192:128–130. [PubMed: 4054313]

31. Nakaie CR, Silva EG, Cilli EM, Marchetto R, Schreier S, Paiva TB, Paiva AC. Synthesis and pharmacological properties of TOAC-labeled angiotensin and bradykinin analogs. Peptides. 2002; 23:65–70. [PubMed: 11814619]

32. Bettio A, Gutewort V, Poppl A, Dinger MC, Zschornig O, Klaus A, Toniolo C, Beck-Sickinger AG. Electron paramagnetic resonance backbone dynamics studies on spin-labelled neuropeptide Y analogues. J Pept Sci. 2002; 8:671–682. [PubMed: 12523644]
33. Smythe ML, Nakaie CR, Marshall GR. α-Helical versus 3_{10}-Helical Conformation of Alanine-Based Peptides in Aqueous Solution: An Electron Spin Resonance Investigation. J Am Chem Soc. 1995; 117:10555–10562.
34. Hanson P, Martinez G, Millhauser G, Formaggio F, Crisma M, Toniolo C, Vita C. J Am Chem Soc. 1996; 118:271–272.
35. Emeis D, Kuhn H, Reichert J, Hofmann KP. Complex formation between metarhodopsin II and GTP-binding protein in bovine photoreceptor membranes leads to a shift of the photoproduct equilibrium. FEBS Letters. 1982; 143:29–34. [PubMed: 6288450]
36. Sakmar TP. Rhodopsin: a prototypical G protein-coupled receptor. Prog Nucleic Acid Res Mol Biol. 1998; 59:1–34. [PubMed: 9427838]
37. Hamm HE, Deretic D, Arendt A, Hargrave PA, Koenig B, Hofmann KP. Site of G protein binding to rhodopsin mapped with synthetic peptides from the alpha subunit. Science. 1988; 241:832–835. [PubMed: 3136547]
38. Dratz EA, Furstenau JE, Lambert CG, Thireault DL, Rarick H, Schepers T, Pakhlevaniants S, Hamm HE. NMR structure of a receptor-bound G-protein peptide. Nature. 1993; 363:276–281. [PubMed: 8487866]
39. Kisselev OG, Kao J, Ponder JW, Fann YC, Gautam N, Marshall GR. Light-activated rhodopsin induces structural binding motif in G protein alpha subunit. Proc Natl Acad Sci U S A. 1998; 95:4270–4275. [PubMed: 9539726]
40. Koenig BW, Kontaxis G, Mitchell DC, Louis JM, Litman BJ, Bax A. Structure and orientation of a G protein fragment in the receptor bound state from residual dipolar couplings. J Mol Biol. 2002; 322:441–461. [PubMed: 12217702]
41. Scheerer P, Park JH, Hildebrand PW, Kim YJ, Krauss N, Choe HW, Hofmann KP, Ernst OP. Crystal structure of opsin in its G-protein-interacting conformation. Nature. 2008; 455:497–502. [PubMed: 18818650]
42. Yang CS, Skiba NP, Mazzoni MR, Hamm HE. Conformational changes at the carboxyl terminus of Galpha occur during G protein activation. J Biol Chem. 1999; 274:2379–2385. [PubMed: 9891006]
43. Oldham WM, Van Eps N, Preininger AM, Hubbell WL, Hamm HE. Mechanism of the receptor-catalyzed activation of heterotrimeric G proteins. Nat Struct Mol Biol. 2006; 13:772–777. [PubMed: 16892066]
44. Martin EL, Rens-Domiano S, Schatz PJ, Hamm HE. Potent peptide analogues of a G protein receptor-binding region obtained with a combinatorial library. J Biol Chem. 1996; 271:361–366. [PubMed: 8550587]
45. Smythe ML, Nakaie CR, Marshall GR. α-Helical versus 3_{10}-Helical Conformation of Alanine-Based Peptides in Aqueous Solution: An Electron Spin Resonance Investigation. J. Am. Chem. Soc. 1995; 117:10555–10562.
46. Mazzoni MR, Malinski JA, Hamm HE. Structural analysis of rod GTP-binding protein, Gt. Limited proteolytic digestion pattern of Gt with four proteases defines monoclonal antibody epitope. J Biol Chem. 1991; 266:14072–14081. [PubMed: 1713215]
47. Kisselev O, Ermolaeva M, Gautam N. Efficient interaction with a receptor requires a specific type of prenyl group on the G protein gamma subunit. J Biol Chem. 1995; 270:25356–25358. [PubMed: 7592699]
48. Papermaster DS, Dreyer WJ. Rhodopsin content in the outer segment membranes of bovine and frog retinal rods. Biochemistry. 1974; 13:2438–2444. [PubMed: 4545509]
49. Hanson SM, Van Eps N, Francis DJ, Altenbach C, Vishnivetskiy SA, Arshavsky VY, Klug CS, Hubbell WL, Gurevich VV. Structure and function of the visual arrestin oligomer. EMBO J. 2007; 26:1726–1736. [PubMed: 17332750]
50. Arimoto R, Kisselev OG, Makara GM, Marshall GR. Rhodopsin-transducin interface: studies with conformationally constrained peptides. Biophys J. 2001; 81:3285–3293. [PubMed: 11720992]

51. Monaco V, Formaggio F, Crisma M, Toniolo C, Hanson P, Millhauser G, George C, Deschamps JR, Flippen-Anderson JL. Determining the occurrence of a 3(10)-helix and an alpha-helix in two different segments of a lipopeptaibol antibiotic using TOAC, a nitroxide spin-labeled C(alpha)-tetrasubstituted alpha-aminoacid. Bioorg Med Chem. 1999; 7:119–131. [PubMed: 10199662]
52. Toniolo C, Valente E, Formaggio F, Crisma M, Pilloni G, Corvaja C, Toffoletti A, Martinez GV, Hanson MP, Millhauser GL, et al. Synthesis and conformational studies of peptides containing TOAC, a spin-labelled C alpha, alpha-disubstituted glycine. J Pept Sci. 1995; 1:45–57. [PubMed: 9222983]
53. Monaco V, Formaggio F, Crisma M, Toniolo C, Hanson P, Millhauser GL. Orientation and immersion depth of a helical lipopeptaibol in membranes using TOAC as an ESR probe. Biopolymers. 1999; 50:239–253. [PubMed: 10397787]
54. McNulty JC, Silapie JL, Carnevali M, Farrar CT, Griffin RG, Formaggio F, Crisma M, Toniolo C, Millhauser GL. Electron spin resonance of TOAC labeled peptides: folding transitions and high frequency spectroscopy. Biopolymers. 2000; 55:479–485. [PubMed: 11304675]
55. Freed, JH. Spin Labeling: Theory and Application. Berliner, LJ., editor. Academic Press; New York: 1976. p. 53-132.
56. Cone RA. Rotational diffusion of rhodopsin in the visual receptor membrane. Nat New Biol. 1972; 236:39–43. [PubMed: 4537062]
57. Heck M, Schadel SA, Maretzki D, Bartl FJ, Ritter E, Palczewski K, Hofmann KP. Signaling states of rhodopsin. Formation of the storage form, metarhodopsin III, from active metarhodopsin II. J Biol Chem. 2003; 278:3162–3169. [PubMed: 12427735]
58. Johnston CA, Siderovski DP. Structural basis for nucleotide exchange on G alpha i subunits and receptor coupling specificity. Proc Natl Acad Sci U S A. 2007; 104:2001–2006. [PubMed: 17264214]
59. Kusumi A, Hyde JS. Spin-label saturation-transfer electron spin resonance detection of transient association of rhodopsin in reconstituted membranes. Biochemistry. 1982; 21:5978–5983. [PubMed: 6295447]
60. Downer NW, Cone RA. Transient dichroism in photoreceptor membranes indicates that stable oligomers of rhodopsin do not form during excitation. Biophysical Journal. 1985; 47:277–284. [PubMed: 3919778]
61. Kisselev OG, Meyer CK, Heck M, Ernst OP, Hofmann KP. Signal transfer from rhodopsin to the G-protein: evidence for a two- site sequential fit mechanism. Proc. Natl. Acad. Sci. U.S.A. 1999; 96:4898–4903. [PubMed: 10220390]
62. Herrmann R, Heck M, Henklein P, Kleuss C, Hofmann KP, Ernst OP. Sequence of interactions in receptor-G protein coupling. J Biol Chem. 2004; 279:24283–24290. [PubMed: 15007073]
63. Arnis S, Hofmann KP. Two different forms of metarhodopsin II: Schiff base deprotonation precedes proton uptake and signaling state. Proc Natl Acad Sci U S A. 1993; 90:7849–7853. [PubMed: 8356093]
64. Mah TL, Szundi I, Lewis JW, Jager S, Kliger DS. The effects of octanol on the late photointermediates of rhodopsin. Photochem Photobiol. 1998; 68:762–770. [PubMed: 9825706]
65. Lewis JW, Szundi I, Kazmi MA, Sakmar TP, Kliger DS. Proton movement and photointermediate kinetics in rhodopsin mutants. Biochemistry. 2006; 45:5430–5439. [PubMed: 16634624]
66. Altenbach C, Yang K, Farrens DL, Farahbakhsh ZT, Khorana HG, Hubbell WL. Structural Features and Light-Dependent Changes in the Cytoplasmic Interhelical E-F Loop Region of Rhodopsin: A Site-Directed Spin-Labeling Study. Biochemistry. 1996; 35:12470–12478. [PubMed: 8823182]
67. Anderson LL, Marshall GR, Baranski TJ. Expressed protein ligation to study protein interactions: semi-synthesis of the G-protein alpha subunit. Protein Pept Lett. 2005; 12:783–787. [PubMed: 16305549]
68. Anderson LL, Marshall GR, Crocker E, Smith SO, Baranski TJ. Motion of carboxyl terminus of Galpha is restricted upon G protein activation. A solution NMR study using semisynthetic Galpha subunits. J Biol Chem. 2005; 280:31019–31026. [PubMed: 15983037]

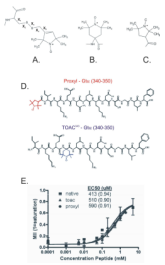

Figure 1. Chemical structures of spin-labels and peptides and the binding of peptides to activated rhodopsin

A. Spin label R1 (cysteine(*S*-(2,2,5,5-tetramethyl-2,5-dihydro-1H-pyrrol-3-yl)methyl-disulfide) used in SDSL with potential degrees of freedom indicated (X_1-X_5 dihedrals). B. TOAC (2,2,6,6-tetramethyl-piperadine-1-oxyl-4-amino-4-carboxyl) spin labels. C. Proxyl (2,2,5,5-Tetramethyl-3-carboxyl-pyrrolidine-1-oxyl) spin label used to modify the amino terminus. D. Chemical structures of two spin-labeled peptides. E. MII stabilization assay for native Gtα(340–350) compared with Proxyl-Gtα(340–350) and $TOAC^{343}$-Gtα(340–350).

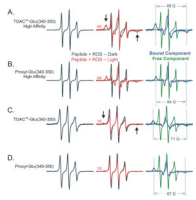

Figure 2. EPR spectra of the indicated spin-labeled peptides

Left hand panel: spectra in the presence of dark-adapted ROS membranes; Center panel: spectra in the presence of photoactivated ROS membranes (red trace) compared to those in the dark-adapted state (black trace); right-hand panel: spectra of the pure bound (blue trace) and unbound (green trace) states obtained by spectral subtraction. The high-affinity peptide data was recorded with 2G modulation amplitude at a temperature of 296° K. The low-affinity TOAC^{343}-Gtα(340–350) and $G_{t\alpha}$(340–350) Proxyl-Gtα(340–350) peptide data was recorded with a 4G modulation amplitude and a temperature of 277° K to facilitate detection of the bound component. The higher modulation accounts for the broader lines in the spectra of the unbound component in (C) and (D). EPR spectra in the left-hand and center panels have been normalized to the same number of spins, and plotted with the indicated scaling factor. Individual component spectra (right-hand panel) are arbitrarily scaled for direct line-shape comparison. The samples were in 20 mM MES buffer (pH 6.8) containing 100 mM NaCl, 2 mM $MgCl_2$, and 10% glycerol.

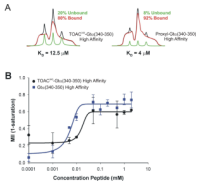

Figure 3. Binding of the high-affinity spin-labeled peptides to photoactivated rhodopsin

(A) Absorption EPR spectra for the TOAC and Proxyl high-affinity peptides in equilibrium with photoactivated rhodopsin at 296° K. The composite absorption spectra (black lines) are shown with the individual spectral components overlaid in green and red. The percentage of rhodopsin-bound peptide was determined by spectral integration. The concentration of rhodopsin and spin-labeled peptide were 90 and 50 μM respectively. The samples were in 20 mM MES buffer (pH 6.8) containing 100 mM NaCl, 2 mM $MgCl_2$, and 10% glycerol. B. Dose-responses of MII formation to determine Kds for $TOAC^{343}$-Gtα(340–350) and Gtα(340–350) high-affinity peptides. The measurements were made independently with different preparation of ROS and the graphs were not normalized to overlap initial and final values.

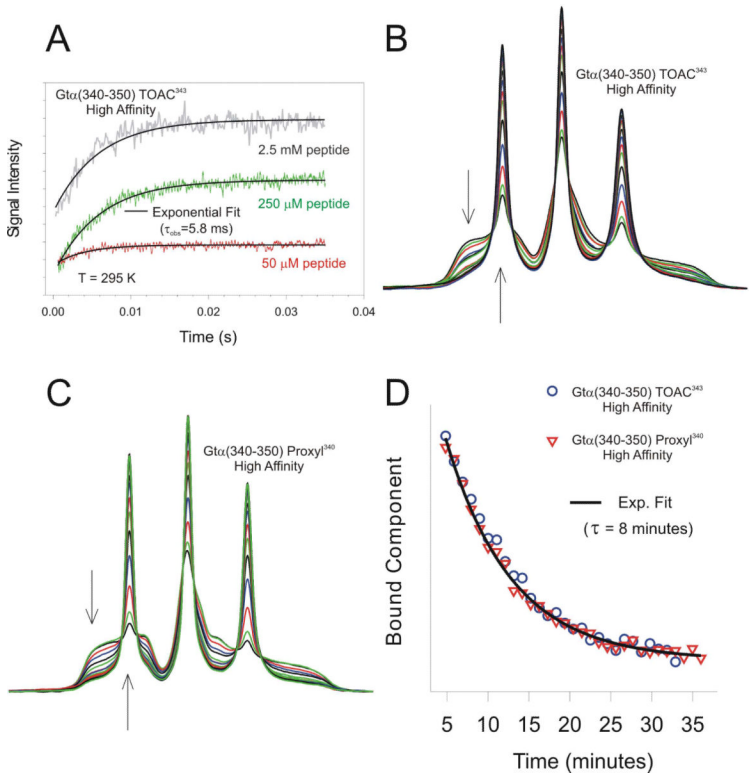

Figure 4. Binding and dissociation kinetics for high-affinity spin-labeled peptides

A) Transient EPR changes for the TOAC^{343}-Gtα(340–350) high-affinity peptide collected at the centerfield trough of the free peptide spectrum are plotted as a function of time after the laser flash. The gray, green, and red traces were collected at peptide concentrations of 2.5 mM, 250 and 50 μM, respectively. The rhodopsin concentration was 250 μM. The samples were in 20 mM MES buffer (pH 6.8) containing 100 mM NaCl, 2 mM $MgCl_2$, and 10% glycerol. All three traces were well fit with a single exponential function with a lifetime of 5.8 ms (black solid lines). B) EPR absorption spectra as a function of time following the rapid transient showing the decay of the immobile spectral component and the appearance of a mobile species for the TOAC^{343}-Gtα(340–350) high-affinity peptide and C, for Proxyl-Gtα(340–350) high-affinity peptides. The arrows indicate the direction of the line-shape changes in time. D) Decay of the bound component with time; blue circles, TOAC^{343}-Gtα(340–350) high-affinity peptides; red triangles, Gtα(340–350) Proxyl-Gtα(340–350) high-affinity peptides. A single exponential (black line) of time constant 8 min was fit to the data.

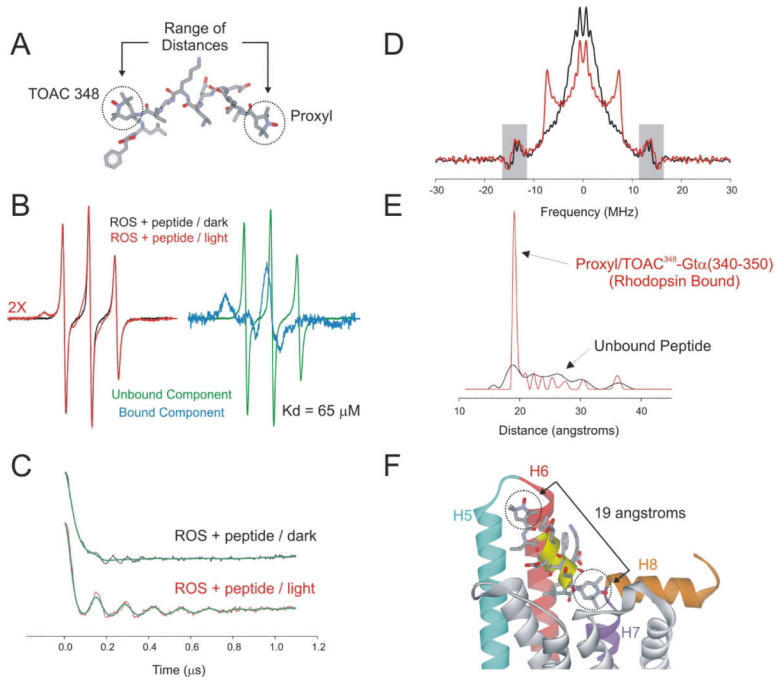

Figure 5. DEER distance measurements for the double spin-labeled peptide Proxyl/TOAC^{348}-Gtα(340–350)

A) Diagram of the high affinity double-labeled undecapeptide. A range of distances between spin labels was anticipated in the unbound peptide in solution; B) Estimation of the dissociation constant of the peptide. EPR spectrum of 90 μM ROS mixed with 50 μM peptide before (black trace) and after (red trace) photobleaching. The individual spectral components were obtained as above, and a Kd of 65 μM was determined. The samples were in 20 mM MES buffer (pH 6.8) containing 100 mM NaCl, 2 mM $MgCl_2$, and 10% glycerol. C) Dipolar evolutions functions for the unbound (black trace) and rhodopsin bound (red trace) peptide. The ROS and peptide concentrations were 250 and 200 μM, respectively. The green traces represent fits to the data using Tikhonov regularization as implemented in the DEER Analysis 2009 software package (see Methods). The high frequency oscillations observed in the unbound peptide dipolar evolution function are electron/proton ESEEM signals that are not fit using the DEER Analysis software package. D) Dipolar spectra of the unbound (black trace) and rhodopsin-bound (red trace) peptide. The gray highlighted regions indicate frequencies where ESEEM signals appear. E) Distance distributions for the unbound (black trace) and rhodopsin-bound (red trace) peptide, and F) Model of the rhodopsin bound double-labeled Proxyl/TOAC^{348}-Gtα(340–350) high-affinity peptide based on the peptide-bound crystal structure of opsin (39). Helix 5, 6, 7, and 8 in opsin are colored cyan, red, purple, and orange respectively. The peptide ribbon is shown in yellow while side chains are shown as sticks. The distance as measured by DEER between the two spin labels matched that predicted from NMR structural data (model not shown) as well as the peptide-bound crystal structure of opsin (39). The Proxyl side chain is more solvent exposed and is projected toward the helix 5/6 loop in opsin, while TOAC-348 is buried near the helix 7/8 interface. Steric contacts between TOAC-348 and opsin likely reduce its binding affinity relative to other spin-labeled peptides (K_d (Proxyl/TOAC^{348}-Gtα(340–350)) = 65 μM).